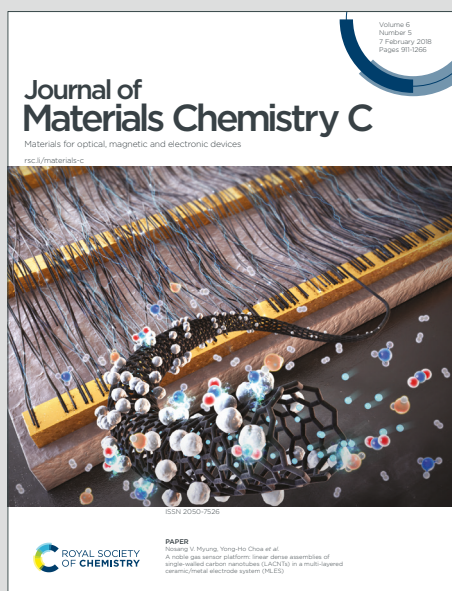


Journal of Materials Chemistry C

Materials for optical, magnetic and electronic devices

Accepted Manuscript

This article can be cited before page numbers have been issued, to do this please use: L. Gutiérrez-Arzaluz, F. López-Salazar, B. Salcido-Santacruz, B. Gonzalez-Cano, R. López-Arteaga, R. O. Torres-Ochoa, N. Esturau-Escofe, F. Cortes-Guzman, R. Martínez and J. Peón, *J. Mater. Chem. C*, 2020, DOI: 10.1039/C9TC05889C.



This is an Accepted Manuscript, which has been through the Royal Society of Chemistry peer review process and has been accepted for publication.

Accepted Manuscripts are published online shortly after acceptance, before technical editing, formatting and proof reading. Using this free service, authors can make their results available to the community, in citable form, before we publish the edited article. We will replace this Accepted Manuscript with the edited and formatted Advance Article as soon as it is available.

You can find more information about Accepted Manuscripts in the [Information for Authors](#).

Please note that technical editing may introduce minor changes to the text and/or graphics, which may alter content. The journal's standard [Terms & Conditions](#) and the [Ethical guidelines](#) still apply. In no event shall the Royal Society of Chemistry be held responsible for any errors or omissions in this Accepted Manuscript or any consequences arising from the use of any information it contains.

ARTICLE

Bisindole Caulerpin Analogues as Nature-Inspired Photoresponsive MoleculesReceived 00th January 20xx,
Accepted 00th January 20xx

DOI: 10.1039/x0xx00000x

Luis Gutiérrez-Arzaluz, Fatima López-Salazar, Bernardo Salcido-Santacruz, Beatriz Gonzalez-Cano, Rafael López-Arteaga, Rubén O. Torres-Ochoa, Nuria Esturau-Escofet, Fernando Cortés-Guzmán, Roberto Martínez* and Jorge Peon*

Photoresponsive molecules are present in many organisms, including animals and plants. These kind of pigments absorb UV or visible radiation and efficiently dissipate the photon energy through pathways that involve intramolecular rearrangements. In this work, a set of bisindole analogs of the natural pigment caulerpin were synthesized and evaluated as photoresponsive systems. The bisindoles of this study are modified versions of the caulerpin metabolite which conserve an asymmetric methinic bridge between two indolyl moieties. In the ground state the more stable conformation for these systems was found to be the E-isomer. Detailed NMR experiments show that upon UVA irradiation (400 nm), the bisindoles evolve to the highly stable Z-isomer which is persistent in solution for several weeks in the dark. Femtosecond resolved measurements revealed a 300 fs deactivation channel for the first singlet excited state which is associated with evolution in the S_1 states leading to ultrafast E-Z photoisomerization and return to the electronic ground state. The excited-state dynamics were also characterized by mapping changes in the electron density in the first singlet excited state. This study shows an evident charge density migration away from the double-bond region upon irradiation. The redistribution of the electron density is followed by a pyramidalization of the adjacent carbon atoms while torsion takes place. The synthesized bisindolic core of this study can lead to the development of novel and easy to functionalize photoresistant and photoresponsive molecules, potentially applicable as photo-controllable molecular switches.

Introduction

Photoresponsive molecules have a prominent role in nature, frequently shielding animal and plant organisms from light-induced damage or performing specific photo-activated roles. This kind of chromophores even includes the DNA bases,¹ and molecules like photoprotective pigments such as melanin,² flavonoids,³ and betalains,⁴ among others.⁵ Within this group of chromophores is caulerpin (see below and Scheme 1). This metabolite is a natural photoprotective pigment present in some genus of algae-like *Caulerpa racemosa* and *Caulerpa serrulata*.⁶ Caulerpin also plays a significant role as a regulator of plant growth,⁷ has antioxidant properties,⁸ and has been shown to have antitumor activity.⁹

The mechanism for the deactivation of many of the natural photoresistant molecules involves significant coupling between the first singlet excited state and the extended potential energy

surface of the electronic ground state.¹⁰⁻¹⁴ Such coupling is frequently associated with an ultrafast excited-state evolution which leads to specific molecular motions upon irradiation which results in the formation of the electronic ground state (with or without isomer formation).^{5, 10, 15, 16} This kind of deactivation pathways uses or dissipates the energy from excitation without any harmful photoproduct release, and can undergo several millions of photo-cycles. These properties make photoprotecting pigments promising photoresponsive molecules and photoswitches.¹⁷ Only a few kinds of deactivation channels are found repeatedly in nature and involve different kinds of molecular motions like excited-state proton transfer,¹⁸ and ring distortions.^{5, 19} Molecules exhibiting conjugated double bonds, like caulerpin, tend to deactivate through the *cis/trans* isomerization coordinate. Among these chromophores are stilbenes,²⁰ rhodopsin,²¹ and azocompounds.²² These kinds of photo-controllable molecules are currently of interest in fields like optogenetics,^{23, 24} photo-controlled drug delivery,²⁵ and as molecular rotors.²⁵

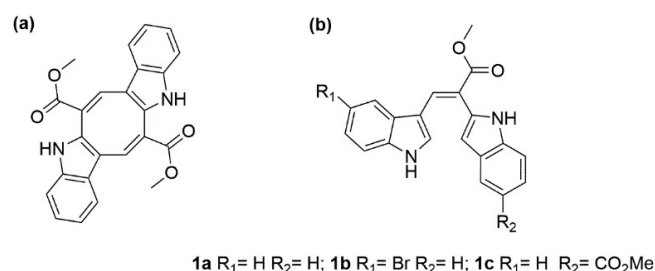
Excited state calculations have been shown to be crucial to understand the ultrafast deactivation of photoprotective and photoswitching molecules, given that detailed knowledge of the excited state pathways can guide the molecular design principles of new systems.^{5, 26, 27} The results obtained from TDDFT,^{28, 29} CASPT2,¹² MR-CI³⁰ approaches indicate that in several cases, the deactivations are mediated by a conical

Universidad Nacional Autónoma de México, Instituto de Química, Ciudad Universitaria, Circuito Exterior, 04510, México.

† Electronic Supplementary Information (ESI) available: Detailed synthetic procedures and characterization from ¹H NMR, ¹³C NMR, IR, and HRMS spectra for all compounds; emission spectra for bi-Br and bi-AcOMe, fluorescence up-conversion transients detecting at 510 nm, calculated vertical excitation energies for bi-Br and bi-AcOMe, potential energy curves for bi-Br, bi-AcOMe and bi-H, NMR characterization for Z-isomer in irradiated sample (¹H, ¹³C, COSY, HSQC, HMBC, and TOCSY spectra), spectral decomposition procedure, isomerization quantum yield calculations, and relevant calculated geometries for bi-H, bi-Br and bi-AcOMe are included. CIF and CCDC compound 1b: 1960596. See DOI: 10.1039/x0xx00000x

intersection (CI) or a progressive reduction of the energy gap between the ground and excited states as a function of a particular molecular coordinate.⁵ The proximity between both states can make the deactivation to occur in an ultrafast and nonradiative fashion. Once back in the electronic ground state, vibrational relaxation takes place within a few picoseconds, which brings the molecule to the lowest vibrational levels of the S_0 surface associated with the respective conformation.

In this work, bisindole molecules inspired on the caulerpin natural product were synthesized and evaluated as photoprotective and photoresponsive systems (see Scheme 1). The bisindoles of our study are built using a methinic group to bridge positions 2 and 3 of two benzopyrrolic systems which can be independently substituted or modified as we show here. From the present results, these systems have photophysical properties which include an ultrafast response through an *E-Z* isomerization channel which occurs with significant photonic yield, and where the photoproduct (*Z* isomer) is stable in the time scale of several weeks in the absence of ambient or sun light. In fact, the photostationary state can be driven to a different relative population of the two isomers depending on the light source, and the relative absorbance of each isomer, but does not evolve thermally (at room temperature), to a different isomer distribution. The influence of substitutions on the indole rings in the photophysics of this core was also explored. Femtosecond resolved measurements, together with TDDFT calculations, indicate that the excited state response is direct and involves a single bright electronically excited state which interacts directly with the ground state surface. These new, easy to functionalize *E-Z* isomerizable systems, which, thanks to the extended conjugation absorb into the visible region, open the possibility of using bisindole-based molecules as photoresponsive molecular switches.



Scheme 1. (a) Structure of Caulerpin. (b) Structure for the molecules studied in this work (bi-H [1a]), (bi-Br [1b]), (bi-AcOMe [1c]).

Results and Discussion

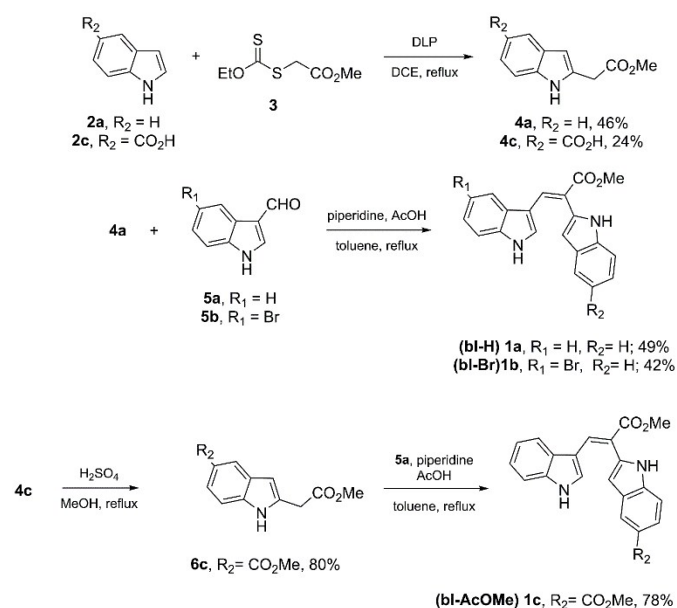
Synthesis.

Compounds **1a-c** (bi-H, bi-Br, and bi-AcOMe) were prepared according to the sequence depicted in Scheme 2. Indoles **2a** and **2b** were first alkylated at the C-2 position in moderate yields by a radical oxidative aromatic substitution reaction with dithiocarbamate **3** following a previously reported procedure.³¹ Then, condensation of **4a** with carbaldehydes **5a** and **5b** was

performed in the presence of catalytic amounts of piperidine and acetic acid to give the bis-indoles **1a** (bi-H) and **1b** (bi-Br) in 49 and 42% yields respectively. In parallel, **1c** (bi-AcOMe) was synthesized in a two steps process including esterification under acidic conditions, followed by a Knoevenagel condensation of the resulting diester **6c** with indole-3-carbaldehyde **5a** (58% over 2 steps). The target molecules were isolated as single *E*-isomers as determined by NMR experiments (COSY, HMBC, 1D-NOESY) and corroborated unambiguously by single-crystal X-ray analysis of compound **1b** (bi-Br) (see Figure S1). Crystallization was attempted for compounds **1a** and **1c** but was unfruitful. Detailed procedures and spectral characterization are included in the ESI.

Steady-State Spectroscopy.

To know the suitability of bisindole derivatives as photoresponsive molecules, absorption and fluorescence spectra were acquired. Steady-state absorption and fluorescence spectra of bi-H, bi-Br, and bi-AcOMe in methanol (HPLC-grade) were acquired in a 1 cm quartz cell in a Cary 50-Bio spectrometer (Varian) and a Cary-Eclipse fluorimeter (Varian) respectively. The fluorescence quantum yields were determined from comparison to Coumarin 102 as reference. The three molecules, bi-H, bi-Br, and bi-AcOMe, were recrystallized before spectroscopic analysis. All experiments were performed at room temperature ($20 \pm 1^\circ C$).



Scheme 2. Synthesis of bisindoles **1a** (bi-H), **1b** (bi-Br), and **1c** (bi-AcOMe). DLP: dilauroyl peroxide, DCE: 1,1-dichloroethane.

The absorption spectra for bi-H, bi-Br, and bi-AcOMe are shown in Figure 1. As can be seen, the three compounds share the same spectral features. bi-H and bi-AcOMe have their lowest energy band at 352 nm and show a shorter wavelength band centered at 275 nm. The bi-Br species has a slight displacement with its bands to 348 nm and 280 nm. These absorption bands

do not correspond with those exhibited by the isolated indole fragment which's characteristic first singlet states band appears at 273 nm.³² Such change in the absorption pattern is indicative of the participation of the double bond bridge in the excitation process, and shows that the system has a much larger conjugation pattern leading to a related bathochromic shift. It is important to note that all three bisindole molecules absorb radiation in the UV-A and UV-B range. This feature is present in many sunscreens, and together with the observed photophysics (see below), makes them attractive candidates as photoprotective compounds.^{5, 10}

Another common characteristic of photoprotective and efficient photoresponsive molecules is a short excited-state lifetime, and the corresponding lack of fluorescence due to the ultrafast nonradiative deactivation of the first excited state.^{11, 20, 22} The bi-H emission spectra in Figure 2 show a faint and broad emission band with a maximum around 400 nm which disappears completely near 600 nm. These broad and weak bands are characteristic of fast deactivation processes involving emission from different points in the excited state surface as relaxation takes place, and the energies of both states (emissive and S_0 state) get closer in energy. Such behaviour has been observed in several systems where the photophysics of the S_1 state is dominated by the presence of a directly accessed conical intersection (CI).^{19, 33, 34} The fluorescence quantum yield for this molecule was found to be $\Phi_F \leq 10^{-4}$, typical of directly accessed non-radiative deactivation pathway which occurs on a much faster time-scale in comparison with the radiative channel.^{20, 30} The bi-Br and bi-AcOMe compounds also present faint emission bands (See Figures S2-S3), and low fluorescence quantum yields ($\Phi_F \leq 10^{-4}$), confirming that the presence of substituents does not affect the spectral properties for these bisindole derivatives.

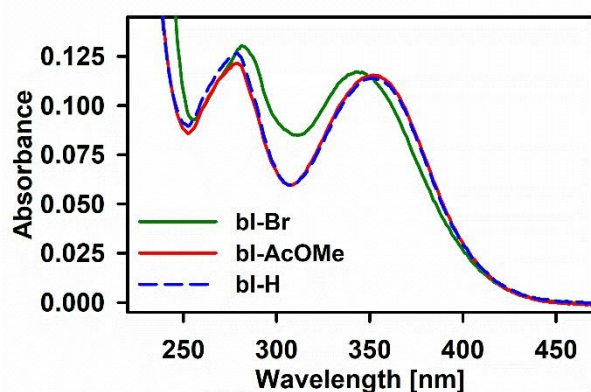


Figure 1. Absorption spectra for bis-indole derivatives in methanol.

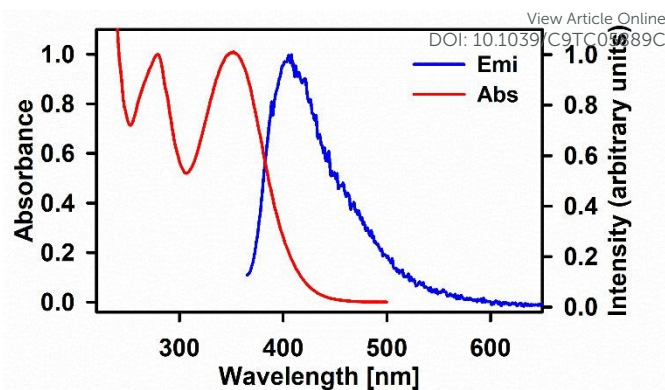


Figure 2. Absorption and emission spectra ($\lambda_{exc} = 350$ nm) for bi-H in methanol. The relative intensities of the emission spectra were independent of the excitation wavelength.

Time-resolved Spectroscopy

Femtosecond time-resolved fluorescence experiments were performed in order to follow the excited state dynamics of the bisindoles directly. The ultrafast molecular dynamics was determined with a femtosecond fluorescence up-conversion setup described in previous contributions.^{35, 36} Briefly, the setup is based on a regeneratively amplified, 1 kHz Ti:Sapphire laser centered at 770 nm producing an 80-fs pulse train. The output pulse was divided into two; the first beam was used to generate second harmonic (385 nm) of the amplified laser in a type-I β -BBO crystal. This 385 nm pulse train was used to excite the sample which was flowing continuously through a 1 mm quartz cell. The resulting fluorescence was collected by a parabolic mirror; any residual excitation energy was eliminated by a long-pass filter. A second parabolic mirror focused the fluorescence in another type-I β -BBO crystal with the time-delayed probe pulse (770 nm). The polarization of the pump pulse was set to the magic angle (54.78°) with respect to the polarization of the gate pulse. The up-conversion signal obtained from the wave mixing was focused to a double monochromator (Oriel) and detected with a photomultiplier tube connected to a lock-in amplifier (Stanford Research Systems) referenced to 1/3 of the laser repetition frequency. The pump beam was modulated by a phase-locked optical chopper at the same frequency with the appropriate phase. The instrument response function (IRF) for the up-conversion experiments was determined from the methanol Raman signal and was Gaussian with a FWHM of 200 fs.

It is known that molecules with low or negligible emission quantum yields can have well-resolved time-gated fluorescence signals for the first few hundreds of femtoseconds upon excitation, since the instantaneous magnitude of these signals only depends on the radiative rate, and not on the overall emission yield.^{30, 37} Additionally, as will be shown in the computational section, these molecules are excited directly to a well-defined bright state. Moreover, our TDDFT calculations show that there are no other dark states between the fluorescent state and the electronic ground state at any conformation (see below). From these considerations, the time-resolved spontaneous emission directly tracks the relevant excited-state evolution.

Figure 3 presents the fluorescence up-conversion transients for bi-H, bi-Br, and bi-AcOMe in methanol detecting at 470 nm and 490 nm. From these results, it can be seen that the three molecules exhibit ultrafast emissive state decays and that the signal has returned to the baseline within two picoseconds. As discussed, with regards to the steady-state spectra, the excited state dynamics of the bisindole molecules is affected only in a minor way by the presence of the attached functional groups, giving the possibility of appending different fragments to the bisindolic core while retaining their photophysical properties. Here, the possibility of functionalizing the CO₂Me groups or constructions through carbon-carbon single bond couplings using the aromatic bromine in bi-Br in one of the chromophores is particularly interesting for future modifications. Also, the same ultrafast deactivation is observed across the emission spectrum of the three molecules (See Figure S4 and Table S1).

As seen in Table 1, the exponential fit parameters for the up-conversion transients reveal a main component with a time constant of less than 300 fs which accounts for the vast majority of the signal amplitude for bi-H and bi-AcOMe. The bi-Br shows a slightly larger time constant ($\tau_1 = 320$ fs). This could be related to the effect of the Br atom size and the respective friction with the solvent molecules.³⁸ The second time constant, around 2 ps, contributes with the remaining small percentage of the amplitude. This component seems to depend on the volume and position of the appending group, with bi-AcOMe having the longest decay time ($\tau_2 = 8.2$ ps). The second component can be explained in terms of different conformations of the *E*-isomer that may be present in the solution as it was found that *syn*- and *anti*- isomers possess somewhat different deactivation rates for methoxycinnamates and urocanic acid sunscreens.^{10, 27} The ultrafast decays of the emissive state are congruent with the photoprotective and photoresponsive purpose, meaning the designed bisindole molecules do conserve the main photophysical properties of caulerpin.

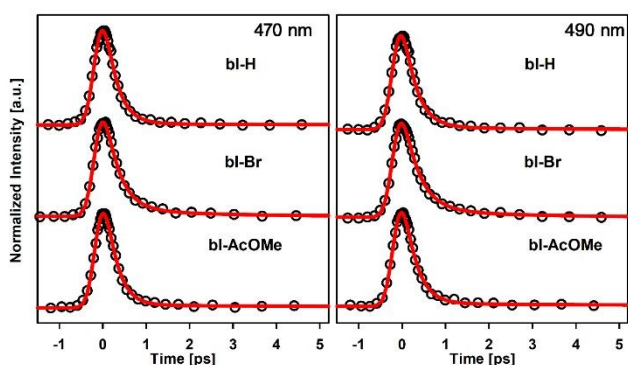


Figure 3. Fluorescence up-conversion transients for bis-indole derivatives in methanol. The pump beam was set at 385 nm, and the emission was monitored at 470 nm and 490 nm. Solid lines indicate the fits for numerically convoluted exponential decays.

View Article Online
DOI: 10.1039/C9TC05889C

Table 1. Fitting parameters for fluorescence up-conversion transients of bisindoles bi-H, bi-Br, and bi-AcOMe in methanol at 470 nm.

	$\lambda_{\text{det}} = 470$ nm				$\lambda_{\text{det}} = 490$ nm			
	α_1 (%)	τ_1 (fs)	α_2 (%)	τ_2 (ps)	α_1 (%)	τ_1 (fs)	α_2 (%)	τ_2 (ps)
bi-H	99.3	270 ± 10	0.7	2.5 ± 0.1	98.5	290 ± 10	1.5	2.2 ± 0.1
bi-Br	95.2	320 ± 10	4.8	2.0 ± 0.1	94.3	350 ± 10	5.7	2.1 ± 0.1
bi-AcOMe	98.7	260 ± 10	1.3	8.2 ± 0.4	98.6	280 ± 10	1.4	7.5 ± 0.2

The ultrafast emissive state decay, together with the significant yield for photoisomerization (see below) can be explained in terms of a direct branched photoinduced isomerization and return to the ground state geometry mediated by a conical intersection (CI).^{11, 28, 30} This phenomenon is typical in several other molecules with a conjugated double bond.^{4, 20, 22} The process is summarized in Figure 4. After excitation, the molecule is promoted to an electronically excited state that undergoes a torsion in the double bond, leading to a loss in the energy of the system. At some point, the energy of the molecule in the excited state nearly or exactly matches with the ground state energy for that geometry, making the deactivation process to continue to the ground state surface where a fraction of the population evolves towards the isomerization channel.

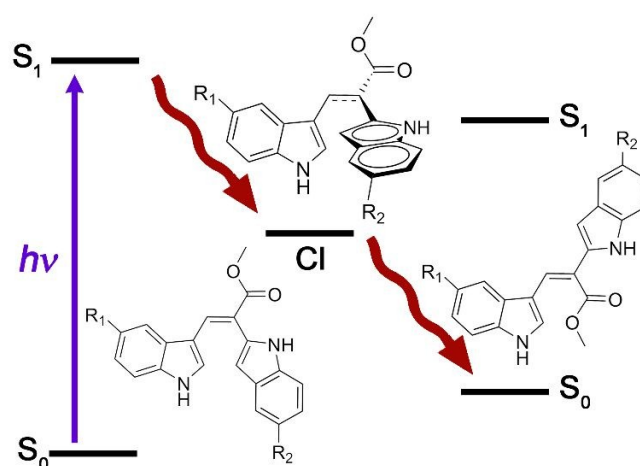


Figure 4. Photoisomerization process in the bisindole derivatives from this study. The structure indicated as CI (Conical Intersection geometry) approximates the molecular structure near the assumed S_1 - S_0 surface crossing.

Photoproduct Characterization.

The photoisomerization process was corroborated for the bisindoles of this study from changes in the absorption spectrum upon irradiation (See Figure 5 for bi-H). The bi-H molecule was irradiated with 5.2 mW of a 405 nm CW laser from PicoQuant (LDH-DC-405) in a 1 cm quartz cell. The changes in the absorption spectrum were monitored as a function of irradiation time. A bathochromic shift, the presence of isosbestic points, and a change in the relative intensity of the absorption bands are observed in the absorption spectrum upon irradiation. As was confirmed through NMR experiments (see below), these changes are associated with the appearance of the Z isomer, which presents absorption bands at longer wavelengths compared to the E form. This is also in accord with our theoretical calculations (see computational section). Taking these results as a starting point, the isolated spectra for each isomer and their changes in concentration were determined following the appropriate calculations (See ESI and Figure S6). The maximum amount of photogenerated Z-isomer is reached after irradiating at 405 nm for 400 s with 5.2 mW beam (absorbance 0.1). Also, from studies of the evolution of the absorption spectra, the photoisomerization quantum yields ($\Phi_{E \rightarrow Z}$) were found to be of up to 7% for the irradiation conditions mentioned before (See a detailed description in the ESI). Crystallization of the Z isomer was attempted but unfruitful.

The produced Z-form does not return to E-isomer within at least several weeks in the absence of room or ambient light, allowing us to perform a full NMR characterization. NMR spectra were acquired in an Avance III HD 700 spectrometer operating at a ^1H frequency of 699.95 MHz (Bruker, Billerica, MA, USA) equipped with a 5-mm z-axis gradient TCI cryoprobe. NMR experiments were recorded using standard Bruker pulse sequences in solutions of bi-H in 5 mm NMR tubes at 298 K.

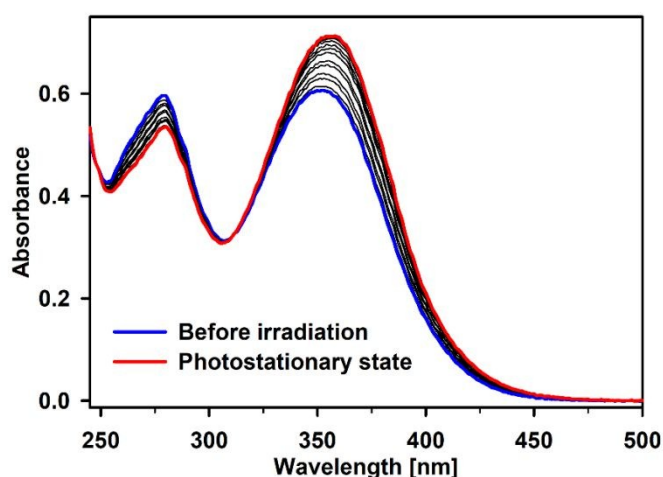
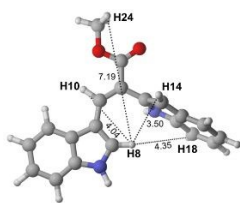
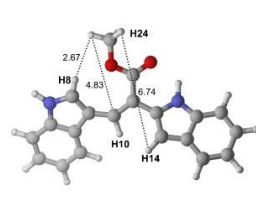


Figure 5. Changes in the absorption spectrum for bi-H in MeOH as a function of irradiation time.

The results found by ^1H , ^{13}C , COSY, TOCSY, HSQC, and HMBC spectra discard any photodegradation or photocleavage of the molecules (See Figures S7-S14). The only signals that increase in intensity after irradiation are the ones corresponding to an isomeric structure (Figure S7). 1D-NMR spectra (Figures S8, S10, S13) confirm the signals with a species with the same number of C and H atoms as the bi-H precursor. 2D-NMR experiments (Figures S9, S11, S12, S14) confirms that the bonding pattern of C and H atoms also resembles the bisindole derivative. Selective 1D-NOESY experiments were used to corroborate the conformational change for bi-H upon 405 nm laser irradiation.

Table 2. Distances in Å for bi-H E and Z isomers and expected NOE signals for both conformations at the CAM-B3LYP/6-311++G(d,p)/PCM: methanol level of theory.

Structure	<i>E</i> -bi-H	<i>Z</i> -bi-H
		
	<i>E</i> -bi-H	<i>Z</i> -bi-H
	Irradiation at H8 frequency	Irradiation at H24 frequency
NOE signals	H8-H10 H8-H14 H8-H18	H24-H8 H24-H10

This kind of NMR experiments allows the observation of H atoms at a spatial distance ≤ 5 Å from another selected H atom. Such information is useful to determine the spatial orientation of different atoms in the molecule. For bisindole derivatives, the change in conformation will result in a change in the NOESY signals that are obtained due to the difference in the relative distances between H atoms in each isomer. Table 2 shows the expected NOE signals established from DFT geometry calculations for E and Z isomers while irradiating at the frequency of a particular H atom. The DFT optimized geometries indicate that there is at least one specific NOE signal to distinguish one isomer from the other, making NOESY experiments suitable to corroborate the photoinduced change in bi-H as an isomerization.

The results for selective 1D-NOESY experiments on bi-H solution before and after laser irradiation are shown in Figures 6 and 7. From Figure 6 it was observed that when selecting the frequency of the H atom in the indole ring (indicated as H8 in Table 2), the NOE signals obtained at 6.41 and 8.38 ppm correspond to the H atoms in the other indole ring and the methinic bridge. These signals with the ground state geometry predicted by the DFT calculations, confirming the E-isomer as the initial species prior irradiation.

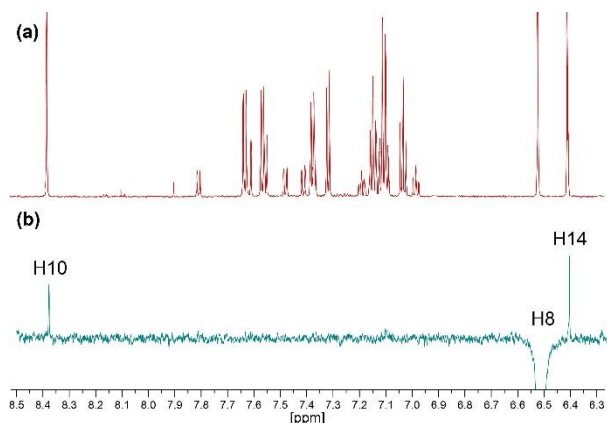


Figure 6. NMR spectra (700 MHz, methanol- d_4 , 298 K) of the irradiated solution ($E:Z$ ratio 4.1:1.0) (a) Conventional ^1H NMR spectrum. (b) Selective 1D-NOESY spectrum using a mixing time of 600 ms. The H8 of E-bi-H was selectively inverted.

On the other hand, when the selected frequency corresponds to the H atoms of the methyl group forming the ester (H24, See Table 2) assigned to the photoproduct, the NOE signals observed in Figure 7 correspond to the Z-bi-H molecule predicted by DFT calculations. The signal at 6.41 ppm is associated to the indole ring (See Table 2), and the one at 7.61 ppm is assigned to the methinic bridge. This evidence confirms the isomerization channel and the respective molecular motions as a consequence of laser irradiation, making the selective switching of the isomers a promising application for bisindoles.

It should be noted that the H8-H18 NOE signal is absent (although an interproton distance of 4.35 Å is predicted by the DFT calculations). This is most likely related to the sensitivity of this distance of the tilt angle of the 2-indole system, which in turn depends on the dihedral angle around the single C-C bond which joins the 2-indole system to the rest of the molecule. In fact, small rotations around this angle reduce the H8-H14 distance as the H8-H18 distance is increased (and vice versa). The presence of a strong NOE signal for the H8-H14 pair seems to indicate a shorter distance for these protons and a longer one for the H8-H18 pair.

Computational Section.

TDDFT calculations were performed in order to characterize the features of the photoisomerization channel as an energetically favoured deactivation pathway and to confirm the absence of other potential channels like crossings into dark electronic states or intersystem crossing. The E and the Z isomer's chemical structures were optimized in their ground state using the X-ray diffraction data of bi-Br (see ESI) as a starting geometry. The calculations were made at the DFT level with the CAM-B3LYP functional³⁹ and the cc-PVTZ Dunning basis set.⁴⁰ Environment effects were taken into account with the PCM model using methanol as solvent.⁴¹

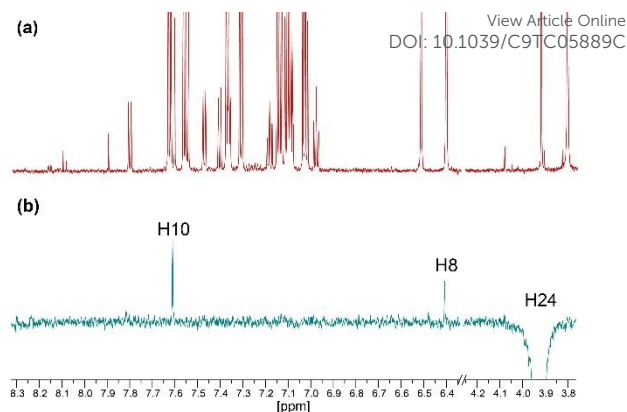


Figure 7. NMR spectra (700 MHz, methanol- d_4 , 298 K) of the irradiated solution ($E:Z$ ratio 4.1:1.0) (A) Conventional ^1H NMR spectrum. (B) Selective 1D-NOESY spectrum using a mixing time of 600 ms. The H24 of Z-bi-H was selectively inverted.

Frequency calculations were achieved to confirm the minima in all molecules for both isomers. The vertical excitation energies were computed at TDDFT/CAM-B3LYP/cc-PVTZ/PCM:Methanol level of theory. The TDDFT approach was chosen due to the size of the system, together with the presence of a large set of nuclear degrees of freedom, making a higher level of theory non-accessible computationally. Furthermore, TDDFT has proven to give good qualitative results for other systems with changes along with the torsional coordinates that lead to conical intersections (CI).^{12, 26, 28, 29, 42, 43} The CAM-B3LYP functional and the consideration of the solvent effects as a dielectric continuum have been also widely used to describe excited state dynamics of conjugated heterocyclic systems.^{39, 44} Finally, partial-optimization scans along $E-Z$ isomerization torsional coordinate for ground and first singlet excited state were made in order to give insights into the excited state deactivation pathways.²⁶ All calculations were performed with Gaussian 09[®] set of packages.⁴⁵

A systematic search for the ground state geometry minima for the bisindole molecules shows the E isomers as the most stable forms in the three derivatives, which is consistent with the observed X-ray structure and the NMR analysis (see Figure S1 and NMR analysis). This conformation can be explained considering the presence of CH- π interaction between bisindole rings (See Figure 8 for bi-H) stabilizing that geometrical arrangement.⁴⁶⁻⁴⁸ Again, bi-Br and bi-ACOMe exhibit similar behavior with a more stable E isomer showing CH- π interaction (See ESI).

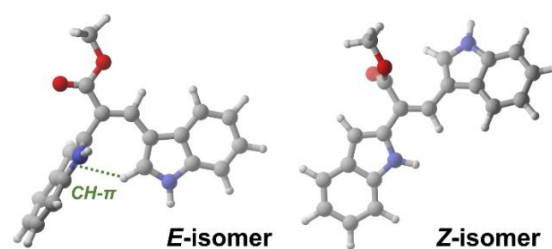


Figure 8. Optimized structures for bi-H E and Z isomers at the CAM-B3LYP/cc-PVTZ/PCM:Methanol level of theory.

ARTICLE

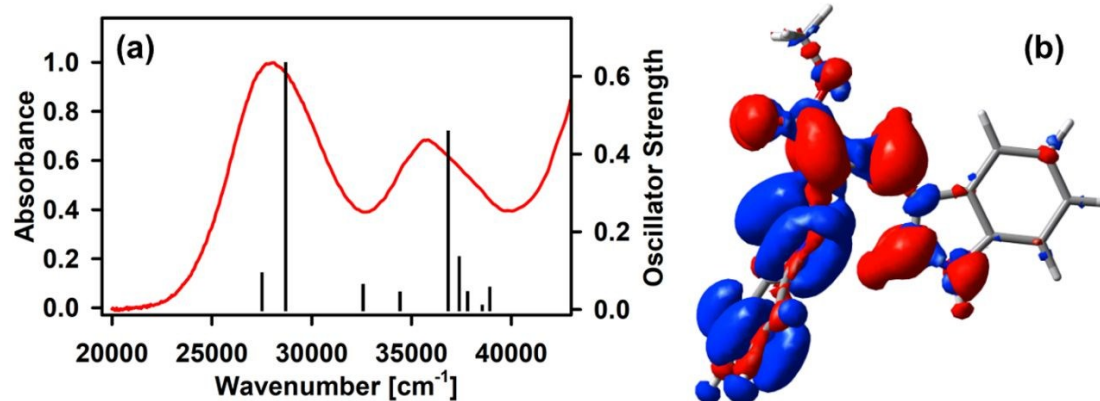


Figure 9. (a) Experimental electronic absorption spectrum for bi-H in methanol (red line) together with calculated oscillator strengths and (b) electron density difference envelopes for the $S_0 \rightarrow S_1$ vertical excitation of bi-H. The values correspond to +0.001 a.u. (red) and -0.001 a.u. (blue). The level of theory used was CAM-B3LYP/cc-PVTZ/PCM:Methanol.

Once the optimized geometries were found, the vertical electronic excitation energies in methanol were computed at TDDFT level for the three compounds, finding excellent agreement with the experimental data (See Figures 9a, S15, and S17, and Tables S4-S6). The results for bi-H in Figure 9a give a good degree of confidence about the excited state surface shapes using this method. From these results, particularly about the identity of the first singlet excited state (accessed with UVA light), and the absence of other states within 0.15 eV above the first singlet, it is clear that our up-conversion experiments with excitation on the edge of the absorption spectrum using at 385 nm pulses selectively lead to the population of the S_1 state. In turn, this is indicative that time constants obtained (Table 1) only involve a direct deactivation to the S_0 state without the involvement of more than one singlet excited state, as mentioned previously.

Another result from the calculations comes from the analysis of the electron density redistribution during the excitation to the S_1 state. Figure 9b displays the changes in electron density for bi-H from the electronic transition, where it can be seen that it involves only one indole ring together with the conjugated double bond and the acetyl group. It is important to underline here that the molecule is not symmetric with regards to the substitution pattern and connectivity of the two heterocycles (see Scheme 1). The electron density redistribution results are congruent with the redshifted absorption wavelengths experimentally found when comparing with the isolated indole chromophore. Also, it is worth to notice

that no n -orbitals from carbonyl group or nitrogen atoms participate in the process as the excitation to S_1 which was found to maintain a π - π^* character across the dynamics (see below). It is noticeable from Figure 9b that some electron density migrates from the double-bond region to the carbon atoms in the bridge. This kind of reorganization is present in other systems that undergo photoinduced E - Z isomerizations.^{43, 49}

The evolution of the energy along the central dihedral torsion coordinate was followed for the S_0 and S_1 electronic states. The scan for bi-H is presented in Figure 10 where it can be seen that the ground state energy sharply rises as the dihedral angle formed by the ring planes is increased, reaching a maximum near 90° . This increase in energy corresponds, in part, to a pyramidalization of the bridge C atoms with a 19° out-of-the-plane angle (Figure 10, right). This geometrical change is characteristic of E - Z and cis - $trans$ rotational photoisomerizations (See ESI).^{29, 49} On the other hand, the S_1 state clearly gets stabilized as the torsion takes place. The decrease in energy leads to significant energetic proximity between the S_0 and S_1 states for this level of theory. Such result strongly suggests a fast excited-state deactivation along isomerization coordinate near 90° . Sufficiently correlated wavefunction methods would likely be able to predict even sharper proximity or a conical intersection for these systems.^{12, 28, 29, 49} The bi-Br and bi-AcOME molecules have the same trend for the energy of both ground and first excited states (Figures S19-S20).

ARTICLE

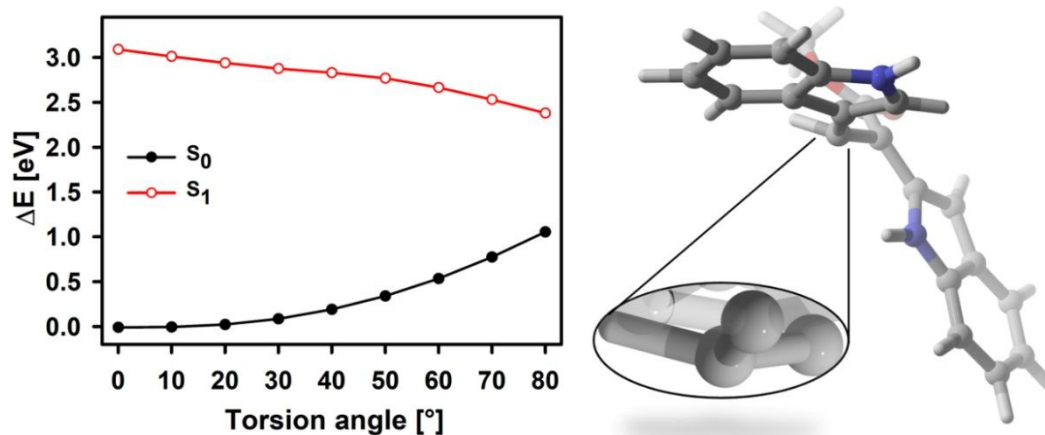


Figure 10. Potential energy curves for ground (S_0) and first singlet excited state (S_1) along isomerization coordinate. Detail of bridge carbon pyramidalization is showed. The level of theory was CAM-B3LYP/cc-PVTZ/PCM:Methanol.

Finally, as a scrutiny exercise, an exploration of the S_2 state in bi-H (Figure S21 and Table S7) revealed that this state is not involved in the torsional deactivation process. Similarly, to the electronic ground state, the S_2 state also destabilizes as the torsion angle increases, making the S_2 and S_1 states to move away in energy. Triplet states T_1 and T_2 were also explored along $E-Z$ isomerization coordinate. These states cannot participate in an intersystem crossing process from the first singlet state since the required energetic coincidence, and transition character (El-Sayed rules) are not fulfilled. This evidence implies that there are not dark singlet state or triplet states involved in the deactivation process

Conclusions

The photophysics of new bisindole-core molecules derived from the natural product caulerpin were studied as photoresponsive molecules. The absorption and fluorescence studies show that these systems are efficient UV-A and UV-B absorbers and photoisomerizable compounds. The $E-Z$ photoisomerization was confirmed by selective 1D-NOESY experiments, confirming a change in the molecular conformation. The time-resolved studies together with TDDFT calculations and irradiation experiments pointed to sub-picosecond deactivation processes ($\tau < 300$ fs) involving $E-Z$ photoisomerization, most likely mediated by a strong S_1-S_0 interaction. Different substitutions on the indole ring do not affect the photoinduced behavior of the bisindolic core. The photostationary state of the bisindole samples is stable for at least several weeks in the dark, implying that the thermal $E-Z$ interconversion is limited by considerable barriers associated with their substitution pattern and other intramolecular interactions. This molecular motif could be used

as new a natural product-inspired building block for photoresponsive systems. In particular, the photostationary states obtained from irradiation of these bisindoles are thermally stable (at room temperature) for at least several days. Such non-reversible systems can have applications in the fields of photopharmacology, light-activated catalysts and organocatalysts, and light-sensitive molecular frameworks, where the desired effect at the molecular level corresponds to a permanent change in the system.⁵⁰

Conflicts of interest

The authors declare no conflict of interest or competing financial interest.

Acknowledgements

Authors acknowledge CONACyT-Mexico grant Fronteras de la Ciencia 179 and PAPIIT/DGAPA/UNAM grant IN208618 and IN208015 for financial support, DGTIC-UNAM project LANCAD-UNAM-DGTIC-210 for computer time. Authors also thank E. Huerta (NMR), A. Peña (NMR), M. P. Orta (IR), L. Velasco, (MS), J. Pérez (MS), C. García (HRMS) and Rubén Toscano (X-Ray) for technical support. This study made use of UNAM's NMR lab: LURMN at IQ-UNAM, which was funded by CONACyT-Mexico (Project 0224747), and UNAM.

References

1. J.-M. L. Pecourt, J. Peon and B. Kohler, *J. Am. Chem. Soc.*, 2001, **123**, 10370-10378.
2. A. Huijser, A. Pezzella and V. Sundström, *PCCP*, 2011, **13**, 9119-9127.
3. N. Saewan and A. Jimtaisong, *J. Appl. Pharm. Sci.*, 2013, **3**, 129-141.
4. A. R. Jiménez and O. Paredes-López, *Crit. Rev. Food Sci. Nutr.*, 2000, **40**, 173-289.
5. L. A. Baker, B. Marchetti, T. N. V. Karsili, V. G. Stavros and M. N. R. Ashfold, *Chem. Soc. Rev.*, 2017, **46**, 3770-3791.
6. K. C. Güven, A. Percot and E. Sezik, *Mar. Drugs*, 2010, **8**, 269.
7. M. F. Raub, J. H. Cardellina and J. G. Schwede, *Phytochemistry*, 1987, **26**, 619-620.
8. C. Kamal and M. G. Sethuraman, *Ind. Eng. Chem. Res.*, 2012, **51**, 10399-10407.
9. P. Yang, D.-Q. Liu, T.-J. Liang, J. Li, H.-Y. Zhang, A.-H. Liu, Y.-W. Guo and S.-C. Mao, *Biorg. Med. Chem.*, 2015, **23**, 38-45.
10. N. D. N. Rodrigues, M. Staniforth and V. G. Stavros, *Proc. - R. Soc. Edinburgh, Sect. A: Math. Phys. Sci.*, 2016, **472**, 20160677.
11. S. Brøndsted Nielsen and T. I. Sølling, *ChemPhysChem*, 2005, **6**, 1276-1281.
12. R. Send and D. Sundholm, *J. Phys. Chem. A*, 2007, **111**, 8766-8773.
13. L. Chen, J. Y. Hu and S. Q. Wang, *Journal of the American Academy of Dermatology*, 2012, **67**, 1013-1024.
14. K. K. Niyogi, *Annual review of plant biology*, 1999, **50**, 333-359.
15. C. E. Crespo-Hernández, B. Cohen, P. M. Hare and B. Kohler, *Chem. Rev.*, 2004, **104**, 1977-2020.
16. C. T. Middleton, K. de La Harpe, C. Su, Y. K. Law, C. E. Crespo-Hernández and B. Kohler, *Annu. Rev. Phys. Chem.*, 2009, **60**, 217-239.
17. F. P. Gasparro, in *Sunscreen Photobiology: Molecular, Cellular and Physiological Aspects*, Springer, 1997, pp. 177-186.
18. J. Zhao, S. Ji, Y. Chen, H. Guo and P. Yang, *PCCP*, 2012, **14**, 8803-8817.
19. A. A. Beckstead, Y. Zhang, M. S. de Vries and B. Kohler, *PCCP*, 2016, **18**, 24228-24238.
20. D. H. Waldeck, *Chem. Rev. (Washington, DC, U. S.)*, 1991, **91**, 415-436.
21. O. Weidlich, L. Ujj, F. Jäger and G. H. Atkinson, *Biophys. J.*, 1997, **72**, 2329-2341.
22. H. Rau, *Angew. Chem., Int. Ed. Engl.*, 1973, **12**, 224-235.
23. K. Deisseroth, *Nat. Methods*, 2010, **8**, 26.
24. O. Yizhar, Lief E. Fenno, Thomas J. Davidson, M. Mogri and K. Deisseroth, *Neuron*, 2011, **71**, 9-34.
25. W. R. Browne and B. L. Feringa, in *Nanoscience and Technology*, Macmillan Publishers Ltd, UK, 2009, DOI: 10.1142/9789814287005_0009, pp. 79-89.
26. C. Ko, J. Quenneville and T. J. Martínez, *Mol. Phys.*, 2006, **104**, 1039-1051.
27. D. Tuna, A. L. Sobolewski and W. Domcke, *J. Phys. Chem. B*, 2014, **118**, 976-985.
28. Y. Harabuchi, S. Maeda, T. Taketsugu, N. Minezawa and K. Morokuma, *J. Chem. Theory Comput.*, 2013, **9**, 4116-4123.
29. N. Minezawa and M. S. Gordon, *J. Phys. Chem. A*, 2009, **113**, 12749-12753.
30. J. P. Villabona-Monsalve, R. Noria, S. Matsika and J. Peón, *J. Am. Chem. Soc.*, 2012, **134**, 7820-7829. New Article Online First Published: 10.1039/C9TC05889C
31. P. E. Reyes-Gutiérrez, R. O. Torres-Ochoa, R. Martínez and L. D. Miranda, *Org. Biomol. Chem.*, 2009, **7**, 1388-1396.
32. X. Meng, T. Harricharran and L. J. Juszcak, *Photochem. Photobiol.*, 2013, **89**, 40-50.
33. D. Onidas, D. Markovitsi, S. Marguet, A. Sharonov and T. Gustavsson, *J. Phys. Chem. B*, 2002, **106**, 11367-11374.
34. J. Peon and A. H. Zewail, *Chem. Phys. Lett.*, 2001, **348**, 255-262.
35. R. López-Arteaga and J. Peon, *J. Phys. Chem. C*, 2018, **122**, 26698-26706.
36. J. Rodríguez-Romero, C. A. Guarín, A. Arroyo-Pieck, L. Gutiérrez-Arzaluz, R. López-Arteaga, F. Cortés-Guzmán, P. Navarro and J. Peon, *ChemPhotoChem*, 2017, **1**, 397-407.
37. R. López-Arteaga, A. B. Stephansen, C. A. Guarín, T. I. Sølling and J. Peon, *J. Phys. Chem. B*, 2013, **117**, 9947-9955.
38. I. B. Berlman, *The Journal of Physical Chemistry*, 1973, **77**, 562-567.
39. T. Yanai, D. P. Tew and N. C. Handy, *Chem. Phys. Lett.*, 2004, **393**, 51-57.
40. T. H. Dunning, *J. Chem. Phys.*, 1989, **90**, 1007-1023.
41. J. Tomasi, B. Mennucci and R. Cammi, *Chem. Rev. (Washington, DC, U. S.)*, 2005, **105**, 2999-3094.
42. L. Gutiérrez-Arzaluz, D. Ramírez-Palma, F. Buitrón-Cabrera, T. Rocha-Rinza, F. Cortés-Guzmán and J. Peon, *Chem. Phys. Lett.*, 2017, **683**, 425-430.
43. L. Gutiérrez-Arzaluz, T. Rocha-Rinza and F. Cortés-Guzmán, *Comput. Theor. Chem.*, 2015, **1053**, 214-219.
44. B. Carloti, F. Elisei and A. Spalletti, *PCCP*, 2011, **13**, 20787-20793.
45. M. J. Frisch, G. W. Trucks, H. B. Schlegel, G. E. Scuseria, M. A. Robb, J. R. Cheeseman, G. Scalmani, V. Barone, B. Mennucci, G. A. Petersson, *et al.*, *Gaussian 09, Revision D.01*, 2016, Gaussian, Inc., Wallingford CT.
46. M. Nishio and M. Hirota, *Tetrahedron*, 1989, **45**, 7201-7245.
47. K. Saigo and Y. Kobayashi, *Chem. Rec.*, 2007, **7**, 47-56.
48. S. Tsuzuki and A. Fujii, *PCCP*, 2008, **10**, 2584-2594.
49. S. Jenkins, L. Blancafort, S. R. Kirk and M. J. Bearpark, *PCCP*, 2014, **16**, 7115-7126.
50. Z. L. Pianowski, *Chemistry—A European Journal*, 2019, **25**, 5128-5144.